Synthesis, oxidation and protonation of octamethyl-1,1′-bipyrrole

Norbert Kuhn,[a]* Heike Kotowski,[a] Manfred Steimann,[a] Bernd Speiser,[b]* Marc Würde[b] and Gerald Henkel[c]

[a] *Institut für Anorganische Chemie, Universität Tübingen, Auf der Morgenstelle 18, D-72076 Tübingen, Germany*
[b] *Institut für Organische Chemie, Universität Tübingen, Auf der Morgenstelle 18, D-72076 Tübingen, Germany*
[c] *Institut für Synthesechemie der Universität-Gesamthochschule Duisburg, Lotharstraße 1, D-47048 Duisburg, Germany*

Received (in Cambridge, UK) 12th July 1999, Accepted 28th October 1999

2,2′,3,3′,4,4′,5,5′-Octamethyl-1,1′-bipyrrole **6** is obtained from 3,4-dimethylhexane-2,5-dione **4** and hydrazine. Treatment of **6** with $[NO]BF_4$ gives the radical cation **11**, while protonation at C_α occurs with HBF_4 to yield the bipyrrolium salt **13**. Oxidation with I_2 results in a bipyrrolium iodide $[\mathbf{6}H^+]\ I_3^- \cdot \frac{1}{2}I_2$ (**14**). The X-ray structures of **6** and **14** are reported.

Electrochemical oxidation of **6** proceeds in two one-electron steps, but is complicated by coupled slow chemical reactions. The oxidized species are stable on time scales shorter than several seconds. The primarily formed radical cation **11**, however, slowly abstracts a hydrogen atom, possibly from the solvent or the supporting electrolyte, to yield protonated bipyrrole **13**. The complex reaction mechanism is supported by electrolysis experiments and simulations of cyclic voltammograms.

Introduction

Surprisingly little attention has been paid to 1,1′-bipyrrole (**1**)

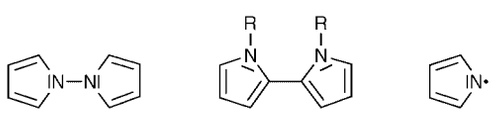

1 **2** **3**

chemistry compared to that of 2,2′-bipyrrole (**2**) analogues.[1] The interest in 1,1′-bipyrroles focuses on the formation of pyrrolyl radicals (**3**)[2–4] as well as on studies concerning their structure and bonding.[5] A special topic deals with the chemistry of hydrazine-bridged annulenes.[6]

As part of our investigations on pyrrolyl and pyrrole metal π-complexes[7] we are interested in reductive N,N-bond fission as a route to new azacyclopentadienyl metal complexes. The properties of 2,2′,3,3′,4,4′,5,5′-octamethyl-1,1′-bipyrrole have been mentioned only briefly.[8] Owing to the remarkable stability of pyrrolyl π-complexes by use of peralkylated azacyclopentadienyl ligands[9] this compound has drawn our attention, and we will report on its synthesis, structure and chemistry in this paper. In particular, its electrochemical oxidation will be described.

Results and discussion

Synthesis and structure of 2,2′,3,3′,4,4′,5,5′-octamethyl-1,1′-bipyrrole

The formation of carboxyalkyl substituted 1,1′-bipyrroles through the stepwise condensation of 1,4-diketones with hydrazine was described many years ago.[10] In addition to the oxidative coupling of alkali metal pyrrolides,[3] this method has been in use up to now.[11]

We have reacted hydrazine with 3,4-dimethylhexane-2,5-dione (**4**) to prepare 2,2′,3,3′,4,4′,5,5′-octamethyl-1,1′-bipyrrole (**6**). No effort has been made to isolate the 1-aminopyrrole **5** which is presumably formed as an intermediate.

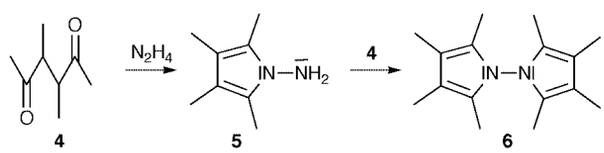

4 **5** **6**

6 has been obtained as colourless crystals in good yield. On comparison with pentamethylpyrrole[12] (^{1}H NMR: δ 3.25, 2.03, 1.80; ^{13}C NMR: δ 121.93, 112.57, 29.55, 9.93, 9.81), no significant differences have been observed in the NMR spectra of **6** (^{1}H NMR: δ 1.98, 1.78; ^{13}C NMR: δ 123.8, 112.5, 10.10, 9.20; see also Experimental part).

Apart from a short remark on the perpendicular orientation of the pyrrole rings in 2,2′,5,5′-tetramethyl-1,1′-bipyrrole (**7**),[13] structural information on 1,1′-bipyrroles is limited to the structure of the trifluoromethylthio derivative **8** (R = SCF_3).[4]

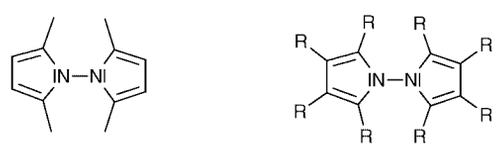

7 **8**

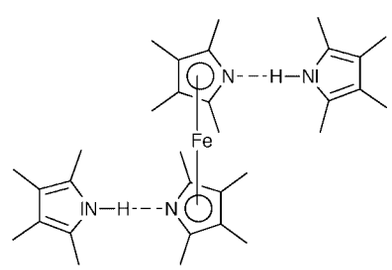

9

Therefore, an X-ray structure analysis of **6** was undertaken. The result (Fig. 1, selected bond lengths and angles in Table 1)

Table 1 Selected bond lengths (Å) and angles (°) of $C_{16}H_{24}N_2$ (**6**)

N(1)–N(2)	1.378(2)	N(1)–C(1)	1.390(2)
C(1)–C(2)	1.360(2)	C(2)–C(3)	1.433(3)
C(3)–C(4)	1.365(2)	N(1)–C(4)	1.379(2)
N(2)–C(9)	1.384(2)	C(9)–C(10)	1.369(2)
C(10)–C(11)	1.428(2)	C(11)–C(12)	1.366(5)
N(2)–C(12)	1.378(2)		
C(1)–N(1)–C(4)	111.0(1)	N(1)–C(4)–C(3)	106.3(1)
C(4)–C(3)–C(2)	108.2(1)	C(3)–C(2)–C(1)	108.2(1)
C(2)–C(1)–N(1)	106.3(2)	N(2)–N(1)–C(1)	124.1(1)
N(2)–N(1)–C(4)	124.6(2)	N(1)–N(2)–C(9)	124.5(1)
N(1)–N(2)–C(12)	124.7(1)	C(9)–N(2)–C(12)	110.9(1)
N(2)–C(12)–C(11)	106.6(1)	C(12)–C(11)–C(10)	108.0(1)
C(11)–C(10)–C(9)	108.1(1)	C(10)–C(9)–N(2)	106.4(1)

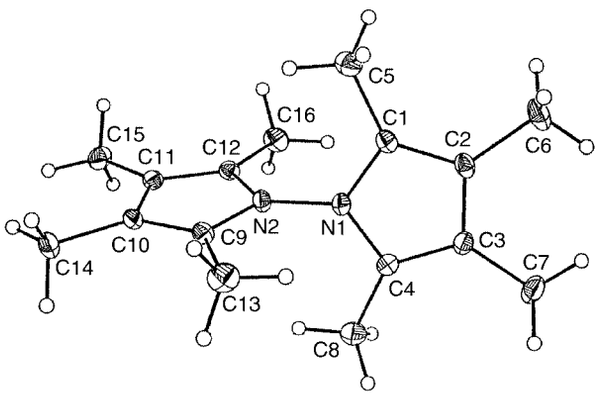

Fig. 1 View of $C_{16}H_{24}N_2$ (**6**) in the crystal lattice.

exhibits an interplanar angle of the pyrrole fragments of 92.4° thus confirming the predictions both of MO calculations and PE experiments.[5] The N,N-distance of 1.378(2) Å lies near the upper end of the range expected for sp^2-hybridized nitrogen atoms. There are no significant differences in the geometry of the five-membered rings (averaged values: N–C_α 1.383, C_α–C_β 1.365, C_β–$C_{\beta'}$ 1.431 Å, C_α–N–$C_{\alpha'}$ 110.9°) as compared to the structure of **9** (averaged values of the uncoordinated pyrrole rings: N–C_α 1.368, C_α–C_β 1.354, C_β–$C_{\beta'}$ 1.425 Å, C_α–N–$C_{\alpha'}$ 109.8°).[14] The molecular geometry of 1,1′-bipyrroles, as indicated by comparison of **6** to published structural data of **8** (R = SCF_3, N–N 1.38 Å, interplanar angle 92.8°) seems to be less influenced by the properties of the substituents.

Chemical oxidation and protonation of 2,2′,3,3′,4,4′,5,5′-octamethyl-1,1′-bipyrrole

The structural relationship between pyrroles and 1,1′-bipyrroles mentioned in the preceding chapter is not confirmed by their chemical properties. In strong contrast to pentamethylpyrrole, **6** is stable to air for some days, and even with respect to its coordination at metal centres we observe a marked decrease in reactivity for the 1,1′-bipyrrole.[15] *In situ* oxidation of pyrroles to pyrrolyl radical cations has been studied extensively to discuss their EPR and UV spectra in the solid state and in solution[13,16–19] in comparison with MO calculations.[20] The EPR spectrum of the 1,1′-bipyrrolylium cation **10** has been

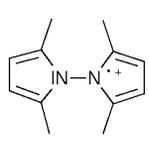

10

mentioned.[13] The reaction of **6** with common chemical oxidants such as ferricenium (fc^+) or silver salts leads to complex mixtures of unidentified products. From **6** and one equivalent of

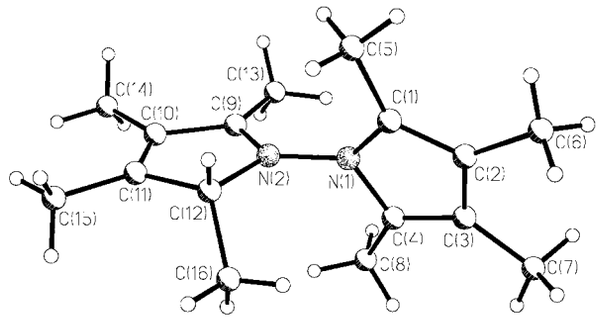

Fig. 2 View of $C_{16}H_{25}N_2I_4$ (**14**, cation) in the crystal lattice.

$NO[BF_4]$ in dichloromethane at 0 °C we obtained a dark red paramagnetic solid whose elemental analysis indicates the composition $C_{16}H_{24}BF_4N_2$ corresponding to the radical salt **11**.

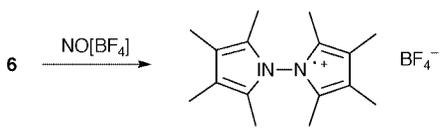

11

From this compound, the 1,1′-bipyrrole **6** is reformed on treatment with magnesium in almost quantitative yield.

The EPR spectrum of **11** exhibits a broad signal (g = 2.0026) both in the solid state and in dichloromethane solution at room temperature. We have not been able to observe hyperfine coupling. Attempts to prepare the dicationic salt **12** through reaction of **11** with a further equivalent of $NO[BF_4]$ failed.

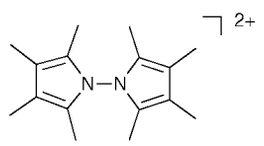

12

Commonly, pyrroles are attacked by electrophiles at the 2-position. Only moderate Brønsted basicity has been mentioned even for alkylated species (pK_a *ca.* 2) and has been investigated extensively in the context of polypyrrole formation.[1,21] Reports on the reaction of 1,1′-bipyrroles as bases are completely absent from the literature, to our knowledge. As a consequence of the substituent effect, we would expect a lower basicity for the bipyrrole as compared to the monocyclic system.

In fact, we could observe protonation of **6** by use of strong Brønsted acids only. The reaction with anhydrous HBF_4 gives the salt **13** as colourless hygroscopic crystals in almost quantitative yield. **13** is only poorly soluble in organic solvents apart

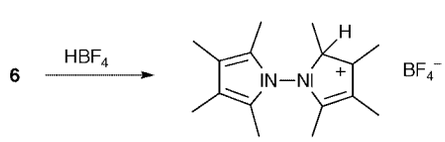

13

from bases like pyridine in which the bipyrrole **6** is reformed. The ^1H NMR spectrum (CD_2Cl_2) exhibits two broad signals at δ 1.72 and 1.90 for the methyl substituents and a sharp singlet at δ 3.53 which we assign to C_α–H.

The X-ray structure analysis of the I_8^{2-} salt **14** obtained from **6** and iodine in acetonitrile clearly confirms the expected protonation at C_α (Fig. 2, selected bond lengths and angles in Table 2). I_2 obviously oxidizes **6** in this reaction. On comparison with the structure of **6**, the N,N-bond is slightly elongated [N(1)–N(2) 1.386(4) Å], and the bond angle of the five-membered ring

Table 2 Selected bond lengths (Å) and angles (°) of $C_{16}H_{25}N_2I_4$ ($\mathbf{14}\cdot\frac{1}{2}I_2$)

Cation			
N(1)–N(2)	1.386(4)	N(1)–C(1)	1.408(6)
C(1)–C(2)	1.355(5)	C(2)–C(3)	1.432(7)
C(3)–C(4)	1.363(6)	C(4)–N(1)	1.396(5)
N(2)–C(9)	1.311(6)	C(9)–C(10)	1.449(6)
C(10)–C(11)	1.338(7)	C(11)–C(12)	1.494(6)
C(12)–N(2)	1.446(5)	C(9)–C(13)	1.469(7)
C(12)–H(12)	0.960	C(12)–C(16)	1.509(7)
C(1)–N(1)–C(4)	109.8(3)	N(1)–C(4)–C(3)	106.7(4)
C(4)–C(3)–C(2)	108.2(3)	C(3)–C(2)–C(1)	108.8(4)
C(2)–C(1)–N(1)	106.3(4)	N(2)–N(1)–C(1)	122.1(3)
N(2)–N(1)–C(4)	123.2(4)	N(1)–N(2)–C(9)	124.4(3)
N(1)–N(2)–C(12)	123.8(3)	C(9)–N(2)–C(12)	111.8(3)
N(2)–C(12)–C(11)	101.5(3)	C(12)–C(11)–C(10)	109.6(4)
C(11)–C(10)–C(9)	108.6(4)	C(10)–C(9)–N(2)	108.6(4)
N(2)–C(12)–C(16)	112.3(3)	C(11)–C(12)–C(16)	118.6(4)
C(16)–C(12)–H(12)	107.9	N(2)–C(12)–H(12)	108.0
C(11)–C(12)–H(12)	107.9		
Anion			
I(1)–I(2)	2.953(1)	I(2)–I(3)	2.892(1)
I(4)–I(4A)	2.768(1)		
I(1)–I(2)–I(3)	178.0(1)		

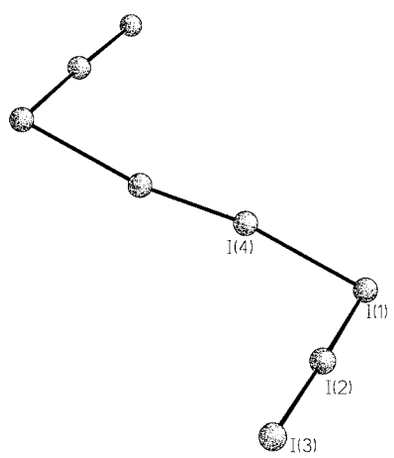

Fig. 3 View of $C_{16}H_{25}N_2I_4$ (**14**, anion) in the crystal lattice.

at the protonated carbon atom is reduced as a consequence of the change in hybridization [C(11)–C(12)–N(2) 101.5(3)°]. The geometry of the I_8^{2-} ion (see Fig. 3) corresponds well to that found in the caesium salt.[22,23]

Electrochemical oxidation of 2,2′,3,3′,4,4′,5,5′-octamethyl-1,1′-bipyrrole

The redox behaviour of **6** was more fully characterized by cyclic voltammetry and electrolysis experiments.

Cyclic voltammetry of 6 on fast time scales. Cyclic voltammograms of **6** in CH_2Cl_2–0.1 M NBu_4PF_6 illustrate the oxidation properties of the 1,1′-bipyrrole. At scan rates up to 10 V s^{-1} two clearly separated peak couples (Fig. 4 for curves recorded at $v = 1$ V s^{-1}) with mid-point potentials of $\bar{E}^{1/4} = +0.489 \pm 0.004$ V (peaks 1 and 4; all potentials referred to the fc/fc^+ standard redox couple[24] in CH_2Cl_2) and $\bar{E}^{2/3} = +0.918 \pm 0.003$ V (peaks 2 and 3) are observed (Table 3). Upon a change in v or c no peaks appear or disappear. Both $\bar{E}$ and the individual peak potentials are independent of v and c with peak potential differences $\Delta E_p^{1/4} = 0.067 \pm 0.008$ V and $\Delta E_p^{2/3} = 0.076 \pm 0.008$ V. These results indicate two reversible one-electron processes. Reversibility of the first electron transfer step is confirmed by the peak current function $i_p^1/\sqrt{v}c$, which is

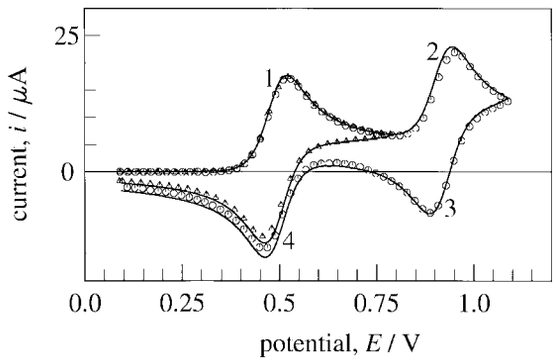

Fig. 4 Experimental (symbols) and simulated (lines) cyclic voltammograms of **6** in CH_2Cl_2–0.1 M NBu_4PF_6, $v = 1$ V s^{-1}, $c = 0.28$ mM, Pt electrode; switching potential $E_\lambda = +0.798$ V, triangles; $E_\lambda = +1.089$ V, circles; simulations calculated under the assumption of two consecutive reversible one-electron transfers.

independent of v and c (Table 4). Under the assumption that peak 1 corresponds to a one-electron step, the voltammetric peak current i_p^1 yields the diffusion coefficient of **6**, $D = 1.09 \pm 0.02 \times 10^{-5}$ cm^2 s^{-1}. For a switching potential of +0.789 V and $v > 0.1$ V s^{-1} the peak current ration i_p^4/i_p^1 is close to unity. At slower scan rates i_p^4/i_p^1 decreases. Thus, on fast time scales the first oxidation process is chemically reversible. On a slower time scale, however, a chemical reaction consumes the first oxidation product. The peak current ratio i_p^2/i_p^1 (for fast v also close to unity; Table 4) confirms that the number of electrons transferred in the first and the second oxidation processes is the same. At slow scan rates, however, i_p^2/i_p^1 increases significantly above 1.

The experimental cyclic voltammograms at scan rates $v > 0.1$ V s^{-1} (symbols in Fig. 4) can successfully be reproduced for switching potentials after the first and second oxidation peak by simulations on the basis of an EE mechanism (solid lines in Fig. 4). This supports the mechanistic hypothesis of a stepwise two-electron oxidation of **6**.

Related, more complex mechanisms may, however, result in similar current/potential curves. In particular, the occurrence of fast and reversible equilibria coupled to the two electron transfer steps may not be distinguished from a simple EE mechanism. Since the product of *chemical* oxidation in CH_2Cl_2 at low temperature could be isolated as the solid radical cation tetrafluoroborate (see above) and this material can be re-reduced to **6**, a hypothetical C-step in an ECE reaction of **6** must leave the bipyrrole moiety intact. Thus, reasonable possibilities for the C-reaction were only a dimerization of the radical cation, or an internal structural rearrangement of this species.

Recently, dimerization of radical ions has been shown to be important in several redox systems.[25] With particular relevance to the present study, a 2,2′-bipyrrole radical cation exhibited a fast reversible dimerization with formation of a σ-bond in solution, and a π-dimer in the crystalline state.[26] Simulations assuming a fast dimerization induced by the one-electron oxidation of **6** suggest that in such a case the mid-point potential calculated from peaks 1 and 4 should depend on the substrate concentration (see also ref. 27). No such effect is, however, observed under our conditions ($0.28 \le c/\text{mM} \le 1.2$), making involvement of dimerization in the present case unlikely.

We therefore describe the oxidation of **6** by two diffusion-controlled one-electron transfer reactions at E^0 (**6**/**11**) = +0.489 V and E^0 (**11**/**12**) = +0.918 V, yielding the radical cation **11** and a dication **12**, respectively (top reactions in Scheme 1). In lieu of direct structural evidence for **11** and **12**, we cannot exclude the possibility of structural rearrangements during the oxidation steps. Any such reactions are thus included in the electron transfer reactions. Both oxidation products are stable on the time scale of the cyclic voltammetric experiments for $v > 0.1$ V s^{-1}.

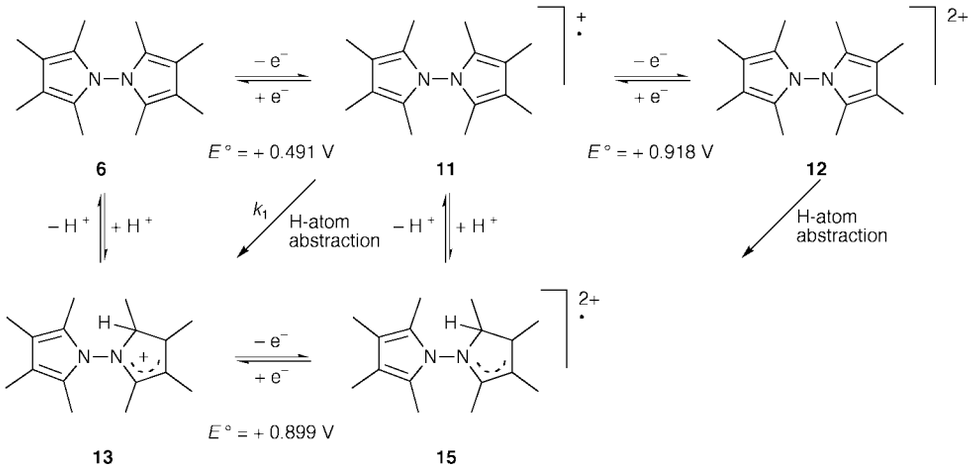

Scheme 1 Oxidation and protonation reactions of bipyrrole **6** as used for cyclic voltammetric simulations; potential values given are those from optimized simulations.

Table 3 Peak potential features[a] in cyclic voltammograms of **6** in CH_2Cl_2–0.1 M NBu_4PF_6

v/V s^{-1}	E_p^1/V	E_p^2/V	E_p^3/V	E_p^4/V	$\Delta E_p^{1/4}$/V	$\Delta E_p^{2/3}$/V	$\bar{E}^{(1/4)}$/V[b]	$\bar{E}^{(2/3)}$/V[b]
0.02	+0.520	+0.955	+0.873	+0.459	0.061	0.082	+0.490	+0.914
0.05	+0.522	+0.955	+0.877	+0.460	0.062	0.078	+0.491	+0.916
0.1	+0.518	+0.950	+0.883	+0.463	0.055	0.067	+0.491	+0.917
0.2	+0.528	+0.961	+0.880	+0.453	0.075	0.081	+0.491	+0.921
0.5	+0.525	+0.952	+0.883	+0.457	0.068	0.069	+0.491	+0.918
1.0	+0.522	+0.949	+0.885	+0.460	0.062	0.064	+0.491	+0.917
5.0	+0.529	+0.962	+0.877	+0.449	0.080	0.085	+0.489	+0.920
10.0	+0.521	+0.957	+0.874	+0.449	0.072	0.083	+0.485	+0.916

[a] For $0.02 \le v$/V s$^{-1} \le 1$: mean values from experiments at three concentrations ($0.21 \le c$/mM ≤ 0.45); for $v > 1.0$ V s^{-1}: $c = 0.12$ mM. [b] Mid-point potentials as mean values of peak potentials associated with the respective redox couple.

Table 4 Selected peak current features[a] in cyclic voltammograms of **6** in CH_2Cl_2–0.1 M NBu_4PF_6

v/V s^{-1}	$i_p^1/\sqrt{v}c^{0}$[b]	i_p^4/i_p^1[c]	i_p^2/i_p^1
0.02	65	0.70	1.28
0.05	63	0.85	1.07
0.1	61	0.90	1.11
0.2	63	0.93	1.08
0.5	63	0.95	1.04
1.0	63	0.96	1.07

[a] Mean values from experiments at three concentrations ($0.21 \le c$/mM ≤ 0.45). [b] In A s$^{1/2}$ cm^3 V$^{-1/2}$ mol^{-1}. [c] For $E_\lambda = +0.789$ V, calculated according to Nicholson.[56]

The difference of the formal potentials for the two redox steps, $\Delta E^0 = E^0$ (**11/12**) $- E^0$ (**6/11**) = 0.429 V, is within the range estimated for two successive electron transfers in an aprotic solvent on the basis of solvation effects in the absence of other factors (0.4–0.5 V).[28] Influences on ΔE^0 have been identified, *e.g.*, solvation,[28] steric strain,[28,29] or substituent effects.[30] Significant structural rearrangements, in particular conformational changes during or accompanying the second electron transfer, often stabilize the two-electron redox product, and in these cases ΔE^0 decreases.[29,31] More closely spaced or even "inverted" formal potentials[31] result ($\Delta E^0 < 0$), but such an effect is not observed in the present system.

The primary oxidation of **6** appears similar to that of hydrazines (for electron transfer reactions of these compounds, see *e.g.* refs. 32–35). It occurs at relatively low potentials, and yields a relatively stable radical cation. On the other hand, however, the oxidation of hydrazines to dications results in very reactive species, whose existence could be proven only under extremely cautious experimental conditions (liquid SO_2 or thoroughly dried CH_2Cl_2 as solvents; low temperatures)[36,37] or with "Bredt's rule protection".[38] In contrast, the two-electron oxidation product of **6** is stable even at room temperature on relatively long time scales ($v \ge 0.1$ V s^{-1}).

As in the case of hydrazines, species **6/11/12** form an open-chain multiple redox system with directly coupled end groups.[39] However, while the nitrogen atoms in hydrazines are of the sp^3-type, in **6** the redox active units are linked by sp^2-N-atoms. Furthermore, in the present case, the N-atoms are part of the five-membered pyrrole rings. In an extension of the recent notation given for radical cations by Schmittel and Burghart,[40] **6** is a π–π system, while a hydrazine would have to be described as n–n. Consequently, it is not surprising that the redox chemistry of **6** is different from that of hydrazine derivatives, and **6** cannot be regarded as a hydrazine. It would be interesting to compare **11** and **12** to hydrazine radical cations and dications, respectively, but due to the absence of structural information about the species in our system, this cannot be attempted as yet.

Compared to **6**, the methoxy substituted 2,2′-bipyrrole described by Merz *et al.*[26] is oxidized at much lower potentials (−0.38 V *vs.* fc/fc$^+$), possibly due to the electron donating substituents. Furthermore, the latter compound attains a co-planar conformation of the two pyrrole rings both in the neutral starting compound and in the radical cation. Thus, delocalization is provided over both heterocyclic rings, while at least **6** has an orthogonal conformation, prohibiting such a stabilizing effect.

Attempts to prepare **12** by chemical oxidation of **6** with two equivalents of NO[BF_4] failed, and only the one-electron oxidation product was isolated. Although the redox potential of the oxidant (≈1.0 V *vs.* fc/fc$^+$ in CH_2Cl_2[41]) is still slightly more positive than E^0 (**11/12**), the E^0 difference is relatively small (<0.1 V), thus probably preventing sufficient oxidation of **11**. Furthermore, as will be discussed below, slow follow-up reactions of **12** could destroy dication formed in such preparative experiments.

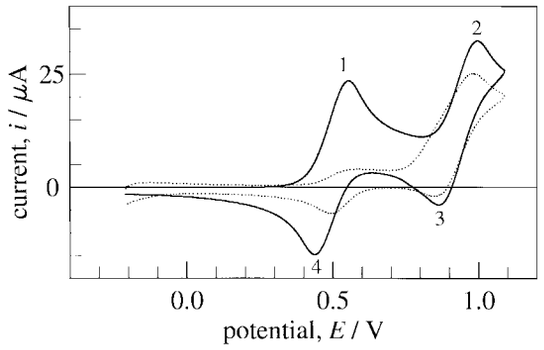

Fig. 5 Experimental cyclic voltammograms of **6** in CH_2Cl_2–0.1 M NBu_4PF_6, $v = 0.1$ V s^{-1}, $c = 1.18$ mM, Pt electrode; before (solid line) and after (dotted line) preparative bulk electrolysis at +0.789 V and passage of a charge corresponding to 1 F.

Cyclic voltammetry on slow time scales and bulk electrolysis of 6. At scan rates below $v = 0.1$ V s^{-1}, the peak current ratio i_p^4/i_p^1 decreases below unity (Table 4), indicating a follow-up reaction of the one-electron oxidation product of **6**, *i.e.* **11**. Such a follow-up reaction is also indicated by a sensitivity analysis of the cyclic voltammetric data.[42] At the same time, however, i_p^2/i_p^1 increases to values above unity. Thus, in peak 2, apart from **11** another species must be oxidized.

In order to determine the nature of the follow-up product, the 1,1′-bipyrrole was oxidized in a potentiostatic bulk electrolysis experiment at a potential $E = +0.789$ V, between peaks 1 and 2 in the cyclic voltammogram of **6**. The current through the electrolysis cell decays initially as usual, but after a charge corresponding to 1 F has passed, it rises again and proceeds through a maximum. The total charge steadily increases. This increase must be due to further electrolysis of products formed from **11** by a slow chemical reaction. We interrupted the electrolysis after a charge corresponding to 8 F had passed through the cell.

If the anodic bulk electrolysis of **6** is stopped at the current minimum (1 F), a deep red solution is obtained. The colour of the solution disappears quickly, and after decoloration, **13** is identified as a reaction product (treatment with NaOH and detection of **6** by NMR). Other products could not be identified in the electrolyte. The electrolyte did not exhibit an EPR signal after decoloration.

In the product solution a cyclic voltammogram was recorded. The current/potential curve (dotted line; Fig. 5) was compared to the voltammogram in the electrolyte before electrolysis (solid line; Fig. 5). Peak 1 has decreased to only a small signal. Consequently, **6** has been consumed almost totally. In the potential range near 0.5 V, the curve is sigmoid rather than peak shaped, indicating a chemical pre-equilibrium to the oxidation of remaining **6**. The second oxidation signal at $E \approx 0.9$ V is broadened and appears to be composed of two strongly overlapping peaks. Peak 3 almost disappears, while peak 4 decreases in intensity and shifts to more positive potentials.

These observations show that on slow time scales the anodic behaviour of **6** is much more complex than the simple stepwise two-electron process found on fast time scales. Additional chemical reactions must at least form the protonated starting compound **13**.

Cyclic voltammetry of 6 in the presence of protons. If the reaction product of the one-electron anodic oxidation of **6** on the bulk electrolysis time scale is indeed the protonated species **13**, voltammograms recorded in solutions of **6** after addition of one equivalent of protons should be similar to those obtained after an electrolysis charge corresponding to 1 F has been passed. Strong acids are necessary to protonate **6** (see above).

Fig. 6a compares cyclic voltammograms of **6** in the absence and presence of HBF_4 at a scan rate of $v = 0.1$ V s^{-1}, scaled to

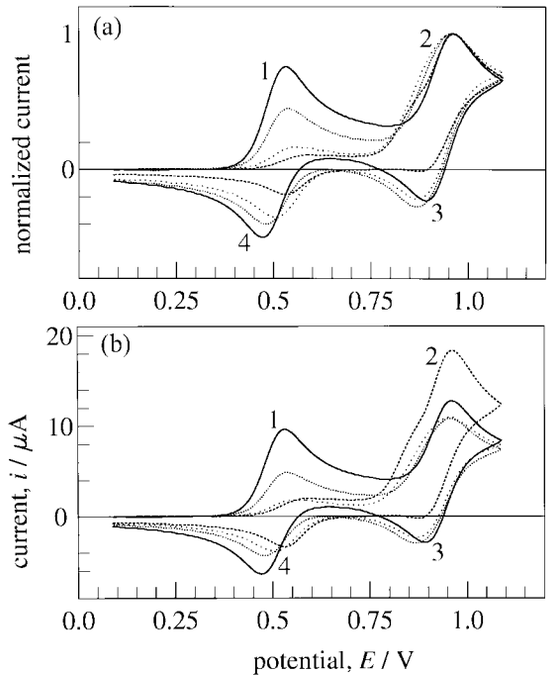

Fig. 6 Experimental cyclic voltammograms of **6** in CH_2Cl_2–0.1 M NBu_4PF_6 with and without HBF_4, $v = 0.1$ V s^{-1}, $c = 0.45$ mM, Pt electrode; added amounts of HBF_4: 0, 0.5, 1.0 and 2.0 equivalents (with decreasing intensity of peaks 1 and 4); a) voltammograms scaled to peak currents of the signal at +0.9 V; b) absolute current values.

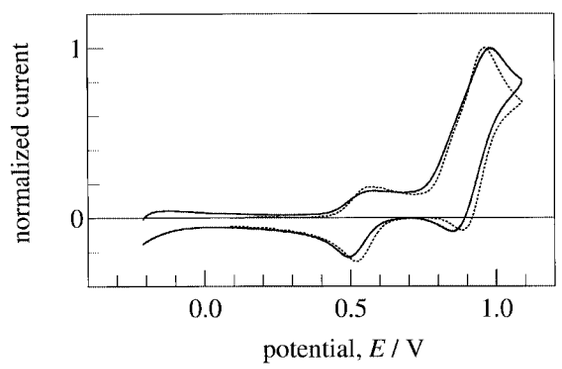

Fig. 7 Experimental cyclic voltammograms of **6** in CH_2Cl_2–0.1 M NBu_4PF_6 after preparative bulk electrolysis at +0.789 V (1 F; $c = 1.18$ mM, solid line) and after addition of 1.25 equivalents of HBF_4 ($c = 0.45$ mM, broken line), scaled to the peak current of the signal at ≈+0.9 V; $v = 0.1$ V s^{-1}.

the respective peak current of the signal at +0.9 V. With an increasing proton concentration, peak 1 in the voltammograms decreases, until a sigmoidal curve remains. At the same time, peak 2 changes its shape and becomes composed of two closely overlapping signals. The absolute, overall intensity of signal 2 (referred to the current decreasing from peak 1 in the respective curve as baseline) increases by a factor of ≈2, until its height is roughly twice that of peak 1 before addition of protons (Fig. 6b). Reduction peak 3 gradually disappears, while suffering a slight shift to less positive potentials. The intensity of peak 4 decreases and it shifts to somewhat more positive potentials upon addition of acid.

Hence, with an increasing amount of protons added, the cyclic voltammograms more and more resemble those recorded in the electrolyte after bulk electrolysis with 1 F. Voltammograms recorded after such an electrolysis and after addition of slightly more than one equivalent of HBF_4 are compared in Fig. 7 (again scaled to the current of the second oxidation peak). Apart from small shifts in the peak potentials (which may be due to some uncompensated *iR* drop in the experiment

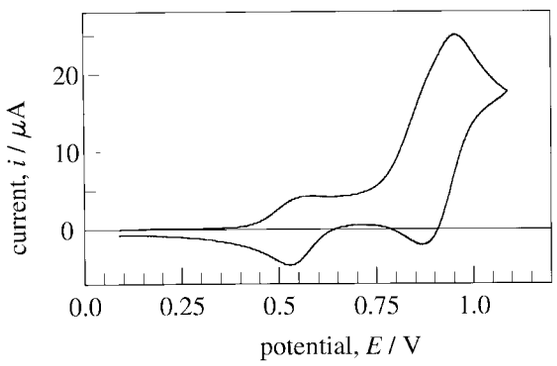

Fig. 8 Experimental cyclic voltammogram of **13** in CH_2Cl_2–0.1 M NBu_4PF_6; $c \approx 0.1$ mM, $v = 0.1$ V s^{-1}.

after electrolysis, performed with a relatively high substrate concentration) the voltammograms are almost identical.

At faster scan rates (above 1 V s^{-1}) the increase of signal 2 upon addition of acid is reduced, and at $v = 20$ V s^{-1} it is larger than peak 1 by a factor of only 1.6. Under such conditions, the peak potential E_p^2 shifts to less positive values (≈30 mV from no HBF_4 to 2 equivalents). Simultaneously, peak 3 remains visible even when protons are present, while the peak shift of signal 4 disappears, and E_p^4 is no longer a function of the amount of protons added. Finally, chemically produced, separately isolated **13** yields similar voltammograms after dissolution in the CH_2Cl_2 electrolyte (Fig. 8). We observe, however, that the current/potential curves recorded in solutions of such samples undergo subtle changes in time. A possible explanation is that the protonation site in crystalline **13** is different from that in solution, but, unfortunately, the low solubility of **13** in CH_2Cl_2 prevents the following of these changes by NMR spectroscopy.

The electrochemical experiments show at least qualitatively, however, that the product of the follow-up reaction of **11** is indeed the protonated form of the starting compound, **13**.

Electrode reaction mechanism for oxidation of 6 under various conditions. In order to reconcile the various mechanistic facets of the anodic oxidation of **6** which emerge from the experimental results, we propose reaction scheme 1.

The neutral starting bipyrrole **6** is oxidized in two one-electron steps *via* **11** to **12**. This simple sequence is observed on fast time scales exclusively (Fig. 4), and has already been discussed above.

If the scan rate in voltammetric experiments is decreased, a follow-up reaction of **11** becomes visible in the current/potential curves (decrease of i_p^4/i_p^1) and the bulk electrolysis experiments show that **13** is the product of the one-electron oxidation of **6**.

The reaction leading from **11** to **13** can formally be interpreted as a hydrogen abstraction by the bipyrrole radical cation from the solvent or the supporting electrolyte. Not many examples of similar reactivity of nitrogen-containing radical cations are provided in the literature. It has, however, been described for intermediates derived from triethylamine[43,44] or 9-arylacridines.[45] In these cases, in contrast to **11**, *N*-protonation was observed. An analogous H-atom transfer is the basis of the Hofmann–Löffler–Freytag reaction.[40]

Species **13** is expected to prevail in the presence of protons, and indeed similar cyclic voltammograms are obtained after electrolysis, addition of a proton acid to the electrolyte, and for isolated **13**.

Protonated bipyrrole **13** forms an acid–base equilibrium with **6**. This reaction explains the sigmoidal shape of the primary oxidation signal in the electrolysed solution,[46] and in solutions of **6** after addition of HBF_4: it acts as a pre-equilibrium to the electron transfer **6**⇌**11** + e^- under conditions where all or almost all **6** has been converted into **13**. The exact protonation site in **13** in solution is not known. However, the X-ray structure of **14** shows protonation at C_α in the solid state and the ^1H NMR spectrum of **13** also indicates C_α-protonation. We thus formulate **13** in a similar way in Scheme 1.

Compounds **6**, **11** and **13** form a cyclic reaction scheme. Oxidation of **6** at the electrode drives this cycle. Such a reaction scheme explains the unusual current/time behaviour during the bulk electrolysis: radical cation **11** formed upon oxidation slowly reacts to **13**, which in turn is in equilibrium with **6**. The latter can again be oxidized, and this process causes the total charge to increase above values expected for a one-electron oxidation if the electrolysis is conducted long enough.

Note that **13** is formed from **6** through initial *oxidation*. This is in full analogy to the formation of **14** from **6** by oxidation with iodine (see subsection Chemical oxidation).

Although **11** decays at small *v* forming **13** with a corresponding decrease of the peak current ratio i_p^4/i_p^1, this is not accompanied by a simultaneous decrease in i_p^2/i_p^1. On the contrary, i_p^2/i_p^1 *increases* with decreasing *v*. A similar observation was made upon protonation of **6** with HBF_4: while peak 1 almost disappears, peak 2 remains present and even increases in intensity by a time scale dependent factor. Thus, on longer time scales the signal at +0.9 V cannot only be attributed to the oxidation of **11** to **12**, but it must also contain contributions from the oxidation of the product formed from **11**. This is in accordance with the fact that it is composed of two closely spaced peaks.

Isolated **13** also shows this signal. This suggests that at +0.9 V not only **11**, but also **13** is oxidized. For the further discussion we assume a one-electron oxidation process of **13** to a hypothetical radical dication **15** (Scheme 1). The potential of the corresponding voltammetric signal is in agreement with the reasonable assumption that the oxidation potential increases going from a species (**6**) to its conjugate acid (**13**). Deprotonation of **15** should lead to radical cation **11**.

At potentials where **13** undergoes oxidation of **15**, **11** can also be oxidized to **12**, which is stable at relatively fast scan rates. The ECE sequence **13**→**15**→**11**→**12** (overall two-electron oxidation) thus explains the occurrence of the rather intense voltammetric signal at +0.9 V under conditions where **13** is the starting species (after electrolysis or isolated **13**).

If the formation of **11** from **15** is fast within the time scale of the experiment (small *v*), the overall electron stoichiometry of the process in signal 2 corresponds to a two-electron process. This explains the increase of the peak current at $E \approx 0.9$ V for $v < 1.0$ V s^{-1} upon addition of HBF_4 to about twice the value of peak 1 in the absence of acid. At larger scan rates the finite kinetics of this reaction results in smaller amounts of **11** being formed. Consequently, less molecules are subject to an overall two-electron oxidation: the current increase of signal 2 upon addition of protons is less pronounced. Less **12** is formed and simultaneously more **15** remains in the vicinity of the electrode.

As suggested by the overlapping peaks in signal 2 and their interpretation as given above, E^0 (**13**/**15**) is slightly less positive than E^0 (**11**/**12**). Thus, the potential shift of the composed signal 2 corresponds to a change from the peak potential of the oxidation current of **11** to that of **13**. This change in the predominant species also explains the potential shift of peak 3 at larger scan rates: the species undergoing reduction becomes mainly **15** rather than **12** under such conditions.

The second reaction cycle with three compounds (**12**, **15** and **11**) in Scheme 1 is responsible for the decrease of the intensity of peak 3 at small *v*. It decreases the concentration of dication **12** in the diffusion layer, as soon as the potential drops below values where this species is produced at the electrode. Fast scan rates work against this depletion and the reduction of **12** can still be observed. This is similar to the behaviour of peak 4 in voltammograms at small *v* and with a switching potential of +0.798 V.

The influence of added protons on the equilibrium between **6** and **13**, *i.e.* a shift to the side of **13**, finally explains the behaviour of E_p^4, as observed in the experiment and mentioned above. An

Table 5 Reaction parameters used to generate optimized simulations of cyclic voltammograms of **6** in CH_2Cl_2–0.1 M NBu_4PF_6

Parameter	Optimized values[a]	
E^0 (**6/11**)	+0.491 V	+0.502 V
E^0 (**11/12**)	+0.917 V	+0.933 V
E^0 (**13/15**)	+0.887 V	+0.899 V
K_1	10^{10} [b]	10^{10} [b]
k_1	0.05 s^{-1}	0.05 s^{-1}
K_2	10^{-3} [c]	10^{-5} [c]
k_2	0.277 M^{-1} s^{-1}	0.8959 M^{-1} s^{-1}
K_3	4927 [d,e]	50.23 [d,e]
k_3	0.5 M^{-1} s^{-1}	19 M^{-1} s^{-1}
K_4	3.2×10^{10} [b,e]	3.8×10^{10} [b,e]
k_4	0.12 s^{-1}	0.122 s^{-1}

[a] Left column: fitting to data from experiment without addition of acid, right column: fitting to data from experiment with addition of acid. [b] Fixed value to model an irreversible reaction step. [c] $K_2 = [\mathbf{6}][H^+]/[\mathbf{13}]$. [d] $K_3 = [\mathbf{11}][H^+]/[\mathbf{15}]$. [e] Thermodynamically superfluous reaction according to ref. 49; value calculated by DigiSim.

increasing proton concentration for a coupled equilibrium of second-order causes a peak potential shift[47] under conditions as found here. Fast scan rates decrease the effect of the coupled chemical reactions and thus the peak shift disappears for large v.

Simulation of cyclic voltammograms of 6 on slow time scales. Recent simulation software[48] for cyclic voltammetric responses allows calculation of theoretical current/potential curves even for complex electrode reaction mechanism such as the one in Scheme 1. However, it is not a simple task to find combinations of parameters which provide meaningful fits between experiment and theory. We adopted a stepwise strategy to determine optimized parameters for the various reactions.

Cyclic voltammograms on fast time scales ($v = 1.0$ V s^{-1}) were successfully simulated taking into account the reaction sequence **6**⇌**11**⇌**12** only (see above and Fig. 4). Heterogeneous rate constants for the electron transfers were assumed well above the reversible limit and the characteristic formal potentials for the two electron-transfer steps used in the calculations [E^0(**6/11**) = +0.491 V and E^0 (**11/13**) = +0.917 V] are close to those derived from the analysis of the experimental peak potentials. The diffusion coefficient for all species was set to $D = 1.09 \times 10^{-5}$ cm^2 s^{-1}, as determined from the peak current data. Analytical concentrations were used throughout. All parameters are given in Table 5.

For scan rates $v \leq 0.1$ V s^{-1}, however, the additional reaction steps derived from the qualitative analysis of the experimental cyclic voltammograms (see previous sections) must be taken into account. In this time regime deviations between the experimental voltammograms and simple EE simulations are observed.

If we assume a first-order follow-up reaction of **11** (Fig. 9a,b) as well as the protonation equilibrium between **6** and **13** (Fig. 9c), the fit between experimental (symbols) and simulated (lines) voltammograms at $v \leq 0.1$ V s^{-1} becomes excellent for $E_\lambda = +0.798$ V. The simulation program employed requires that chemical reactions are formulated as equilibria. In order to model the assumed irreversibility of the hydrogen abstraction step **11**→**13**, we set the equilibrium constant K_1 to large values (10^{10}). A series of calculations shows that the exact value of K_1 does not influence the resulting current/potential curve to a significant extent. All other kinetic parameters were optimized to fit the present data set as close as possible.

In order to model the current/potential curves with a switching potential of $E_\lambda = +1.089$ V at $v \leq 0.1$ V s^{-1}, further reaction steps were introduced into the simulations. Consideration of the redox reactions corresponding to the oxidations of **11** and **13** only (again with high heterogeneous electron transfer rate constants) yields voltammograms with strong deviations close to peaks 2 and 3. However, taking into account the deprotonation **15**→**11** + H^+ and, in particular, a hydrogen abstraction reaction similar to that leading from **11** to **13**, but with **12** as the starting species and producing **15**, we achieve good quality fits between experiments and simulations (Fig. 9d–f). Again, the equilibrium and rate constants were optimized if necessary. It is important to note that K_3 and K_4 for the two additional chemical reactions are set to fixed values by the simulation program, due to the fact that in our reaction scheme the corresponding equilibria are regarded as "thermodynamically superfluous reactions" (TSR).[49]

The reaction parameters used to calculate the optimized simulations for various scan rates and switching potentials (Table 5) fit into the picture that we have already presented for the oxidation of **6**. All chemical reactions are relatively slow, in accordance with the fact that voltammograms at $v > 0.1$ V s^{-1} can be described by a simple EE model. The value of E^0 (**13/15**) differs from E^0 (**11/12**) by only 30 mV, accounting for the closely overlapping peaks in signal 2. The TSR based equilibrium constants have reasonable values in view of an expected acidic dication radical **15** and the expected irreversibility of hydrogen abstraction by **12**. The latter reaction step appeared to be essential in order to fit the voltammogram at $v = 0.02$ V s^{-1} with the extended potential scan range in Fig. 9f. It might explain our failure to generate **12** from **6** by chemical oxidation, and possibly indicates that **12** might possess the properties of a triplet biradical. Proof must, however, be left to separate work.

Finally, simulation of the cyclic voltammograms obtained in the presence of acid was attempted with the reaction model acquired so far. The numerical values of the reaction parameters had to be adjusted slightly in order to fit the experimental data, which were taken from a fully independent cell set-up as compared to the experiment discussed above. The quantitative agreement between experimental and simulated curves in this more complex case was less satisfactory. However, a qualitative comparison (see Fig. 10 for a selection of voltammograms at $v = 0.02$ V s^{-1} and various proton concentrations) shows that the model employed does indeed correctly predict the changes in curve shape upon addition of protons which have been discussed previously.

Thus, the simulations of voltammograms on slow time scales support the reaction mechanism derived for the anodic oxidation of **6** in the previous sections.

Conclusion

The synthesis of 2,2′,3,3′,4,4′,5,5′-octamethyl-1,1′-bipyrrole (**6**) proceeds starting from hydrazine and 3,4-dimethylhexane-2,5-dione in good yield. Its structure confirms the small influence of the π-electron distribution on the geometry of the ring fragments whose planes are oriented almost perpendicularly. Nevertheless, we observe a drastic decrease in reactivity towards electrophiles compared to pentaalkylpyrroles. In contrast to pentamethylpyrrole, **6** is stable to air, and oxidation needs strongly oxidizing reagents like $[NO]BF_4$. As mentioned for pyrroles, protonation occurs at the α-position, but, in contrast to 2,3,4,5-tetramethylpyrrole, we have not been able to characterize the bipyrrolium salt **13** spectroscopically in solution apparently as a consequence of its low solubility in non-basic solvents.

Several attempts to prepare metal pyrrolides from **6** and metal carbonyls failed and are not discussed in detail here. The formation of sodium pyrrolide on reacting **6** and sodium even under drastic conditions could not be detected. Apparently, N,N-bond weakening by electronic repulsion as discussed for hydrazine is not predominant here presumably as a consequence of the incorporation of the nitrogen lone pairs into the heteroaromatic 6π-electron systems.

Electrochemical data of **6** could be measured and simulated

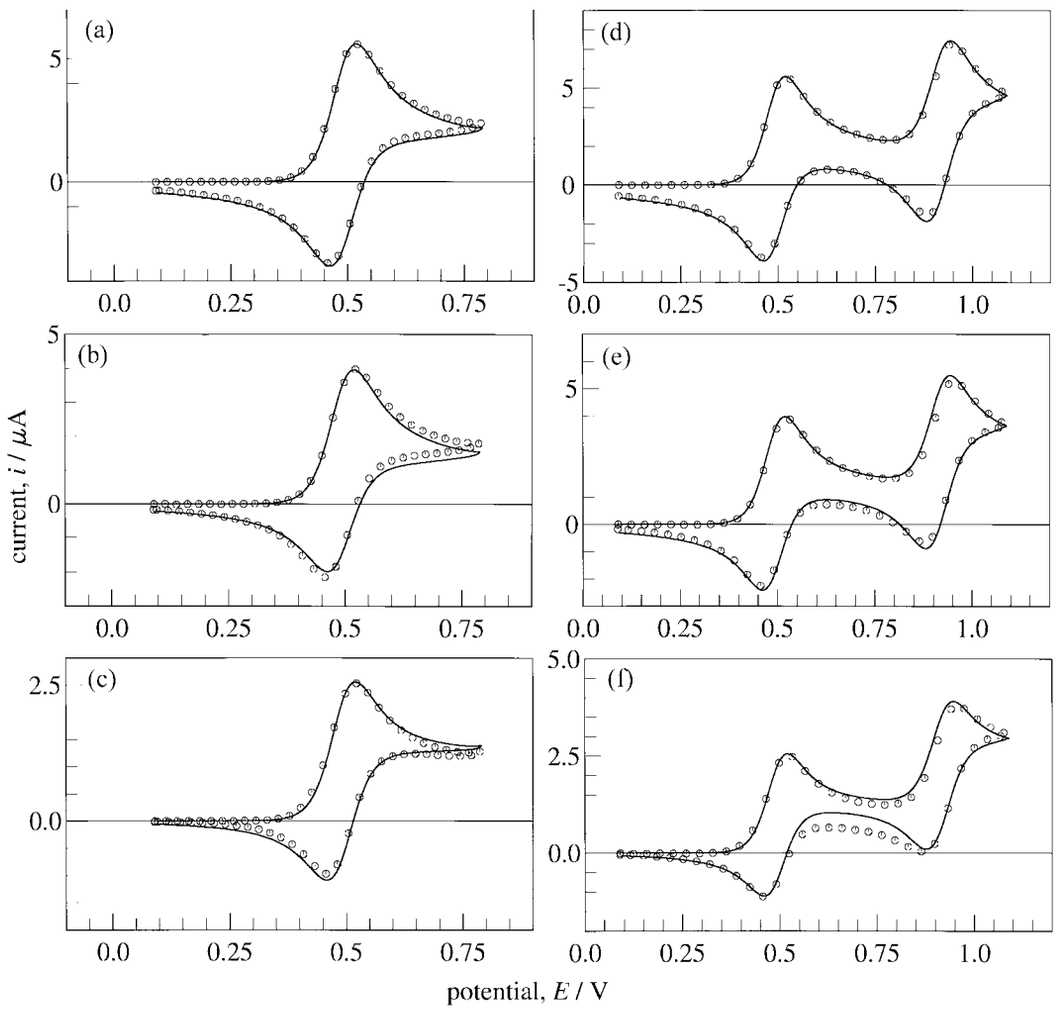

Fig. 9 Experimental and simulated cyclic voltammograms of **6** in CH_2Cl_2–0.1 M NBu_4PF_6 on slow time scales; $c = 0.28$ mM; a)–c): $E_\lambda = 0.798$ V, d)–f): $E_\lambda = 1.098$ V; a), d): $v = 0.1$ V s^{-1}, b), e): $v = 0.05$ V s^{-1}, c), f): $v = 0.02$ V s^{-1}; for mechanistic models used, see text.

under a large variety of experimental conditions (scan rates, concentrations, proton concentrations, starting species), thus enabling a detailed analysis of the complex reaction scheme. At the electrode, **6** can be oxidized in two separate one-electron steps. On slow time scales the electrode reaction is complicated by several coupled chemical reactions. The one-electron oxidation product of **6**, *i.e.* **11**, provides another example of a nitrogen containing radical cation, which stabilizes itself by abstraction of a hydrogen atom. This reaction is the key step in the explanation of the qualitative and quantitative features of the cyclic voltammograms and electrolysis experiments. **6** appears as an open-chain multiple redox system with directly coupled end groups,[39] similar to hydrazines, for example. In contrast to the latter, however, the bipyrrole system is of the π–π type in the Schmittel–Burghart notation,[40] which might account for its deviating chemical and electrochemical reactivity.

Experimental

General

All synthetic experiments were routinely carried out in purified solvents under argon. 3,4-Dimethylhexane-2,5-dione (**4**)[50] was prepared according to published procedures.—NMR spectra: Bruker DRX 250.—EPR spectra: Bruker ESP 300E.—Mass spectra: Varian MAT 311A.

Syntheses

2,2′,3,3′,4,4′,5,5′-Octamethyl-1,1′-bipyrrole, 6. 3.56 g (71 mmol) of anhydrous hydrazine were added to a solution of 20.22 g (142 mmol) **4** in 30 ml glacial acetic acid at 5 °C in the course of 5 min. After stirring for 12 h at room temp., 300 ml of water were added, and the mixture was stirred for a further 2 h. The precipitate was isolated, washed with water and dried *in vacuo* to yield **6** as colourless crystals (13.72 g, 79%), mp 127–128 °C. Calc. for $C_{16}H_{24}N_2$: C, 78.64; H, 9.90; N, 11.46. Found: C, 78.59; H, 9.98; N, 11.36%. δ_H (C_6D_6, 250.13 MHz, TMS int.) 1.98 (6 H, s, 2,2′,5,5′-CH_3), 1.78 (6 H, s, 3,3′,4,4′-CH_3). δ_{u_C} ^{13}C NMR (C_6D_6, 62.90 MHz, TMS ext.) 123.8 (C-2,2′5,5′), 112.5 (C-3,3′,4,4′), 10.10 (2,2′,5,5′-CH_3), 9.20 (3,3′,4,4′-CH_3). *m/z* (70 eV, EI; %) = 244 [M^+], 29), 122 ([$M^+ - C_8H_{12}N$], 100).

2,2′,3,3′,4,4′,5,5′-Octamethyl-1,1′-bipyrrolium radical cation tetrafluoroborate, 11. 0.239 g (2.05 mmol) $NO[BF_4]$ were added to a solution of 0.501 g (2.05 mmol) **6** in 30 ml dichloromethane at 0 °C in the course of 5 min. After stirring for 12 h at room temp. the filtered solution was evacuated to dryness, and the remaining residue was washed with 20 ml *n*-pentane over a period of 30 min to yield a dark red solid (0.628 g, 92%), mp (dec.) 119–122 °C. EPR (CH_2Cl_2 at room temp., *vs.* 2,6-di-*tert*-butyl-3,5-di-*tert*-butoxyphenoxyl [$g = 2.004627$]): $g = 2.0026$. Calc. for $[C_{16}H_{24}N_2]BF_4$: C, 58.03; H, 7.30; N, 8.46; F, 22.95. Found: C, 57.65; H, 7.38; N, 9.06; F, 23.40%.

2*H*-2,2′,3,3′,4,4′,5,5′-Octamethyl-1,1′-bipyrrolylium tetrafluoroborate, 13. 0.52 ml HBF_4 (54% solution in diethyl ether) were added to a solution of 0.934 g (3.82 mmol) **6** in dichloromethane at −20 °C. After warming up to room temp. in the course of 30 min, the solid was isolated, washed repeat-

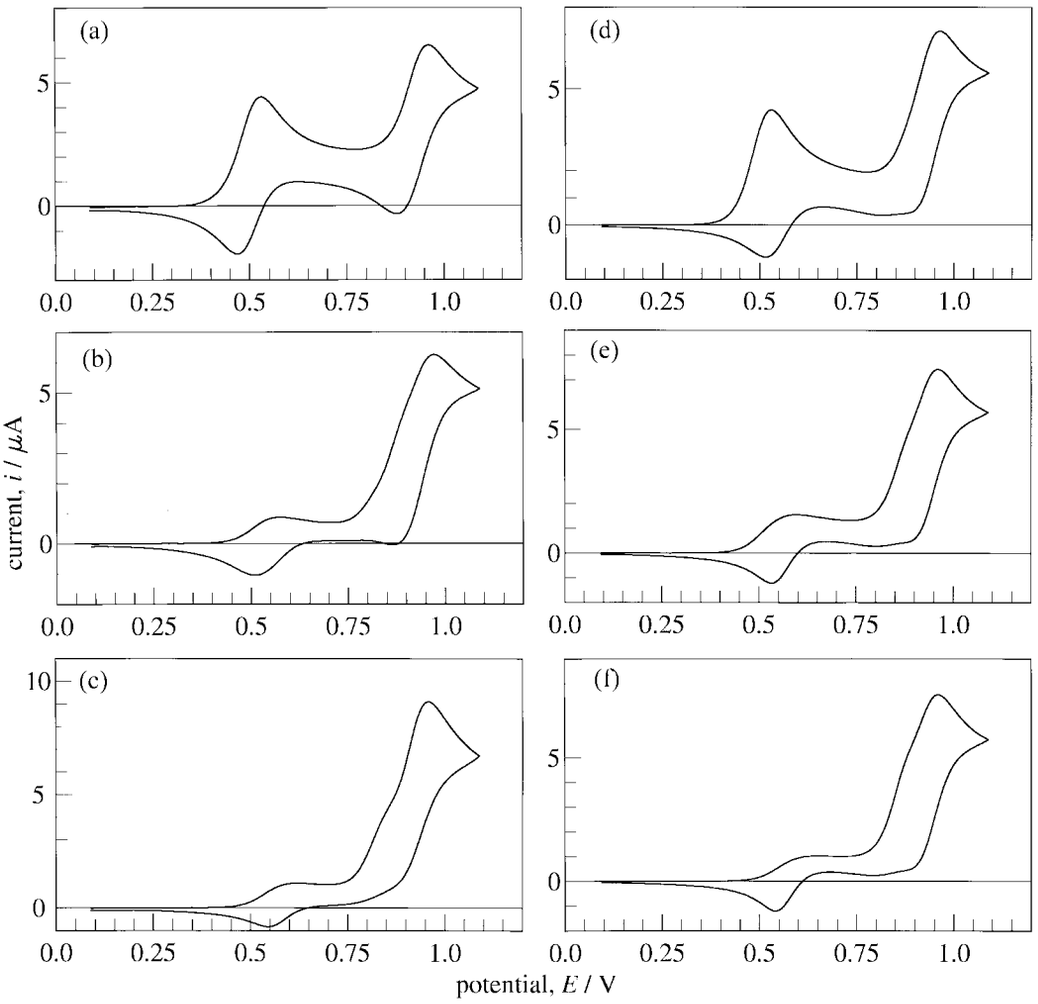

Fig. 10 Experimental (a–c) and simulated (d–f) cyclic voltammograms of **6** in CH_2Cl_2–0.1 M NBu_4PF_6 in presence of HBF_4; $c = 0.47$ mM; $v = 0.02$ V s^{-1}; proton concentrations $c(H^+) = 0.0$ (a, d), 0.45 (b, e), 0.9 (c, f) mM; simulation parameters, see Table 5.

edly with dichloromethane and dried *in vacuo*. Yield 1.02 g (80%), colourless solid. ^{1}H-NMR (CD_2Cl_2, 250.13 MHz, TMS int.): $\delta = 3.53$ (s, 1 H, C_α-H); 1.90, 1.72 (2 br s, 24 H, CH_3). $[C_{16}H_{25}N_2]BF_4$ (332.18): Calc.: C, 57.85; H, 7.59; N, 8.43; F, 22.88. Found: C, 57.15; N, 7.90; N, 8.01; F, 22.13%.

Crystal structure analysis of 6.† $C_{16}H_{24}N_2$, $M = 244.37$ g mol^{-1}, $T = 173$ K, crystal dimensions *ca.* $0.30 \times 0.25 \times 0.25$ mm, Siemens P4 four circle diffractometer, μ(Mo-Kα) = 0.063 mm^{-1}, graphite monochromator, orthorhombic, cell dimensions $a = 8.420(1)$, $b = 16.681(3)$, $c = 21.656(5)$ Å, $U = 3042(1)$ Å^3, space group *P*bca, $Z = 8$, $D_c = 1.067$ g cm^{-3}, $F(000) = 1072$. Data collection: $2\Theta = 4$–50° (8.37–29.30° min^{-1}), $\bar{\omega}$-scan, 10124 reflections collected, 2678 independent reflections ($R_{int} = 0.0429$) with $I > 2\sigma(I)$; direct methods, full matrix least-square refinements, non-hydrogen atoms anisotropic, H atoms at idealized positions, SHELXTL V5.1 (NT), *R* indices (all data): $R1 = 0.0645$, $wR2 = 0.1043$, final *R* indices [$I > 2\sigma(I)$]: $R1 = 0.0366$, $wR2 = 0.0930$, 164 parameters, *GooF* 1.281.

Crystal structure analysis of 14.† $C_{16}H_{25}N_2I_4$, $M = 752.98$ g mol^{-1}, triclinic, space group $P\bar{1}$, $a = 8.376(3)$, $b = 11.618(5)$, $c = 12.271(4)$ Å, $\alpha = 86.16(3)$, $\beta = 84.31(3)$, $\gamma = 72.48(3)$°, $U = 1132.25$ Å^3, $Z = 2$, $D_c = 2.209$ g cm^{-3}, μ(Mo-Kα) = 5.50 mm^{-1}, Siemens P4RA four circle diffractometer, rotating anode generator, Mo-Kα radiation ($\lambda = 0.71073$ Å), graphite monochromator, scintillation counter, $T = 150$ K, empirical absorption corrections, direct methods, full matrix least square refinements, non-hydrogen atoms isotropic, H atoms at idealized positions, one common isotropic temperature factor for H within each residue, one extinction parameter, one scaling factor, transmission range 0.995–0.308, $2\Theta_{max} = 54°$, $\bar{\omega}$ scan, crystal dimensions *ca.* $0.55 \times 0.23 \times 0.12$ mm, 4940 unique reflections, $R(R_w) = 0.0310(0.0382)$ for 4529 reflections with $I > 2\sigma(I)$, 209 variables.

† CCDC reference number 188/201. See http://www.rsc.org/suppdata/p2/a9/a905603c for crystallographic files in .cif format.

Electrochemical experiments

Dichloromethane was predried over $CaCl_2$. It was distilled from P_2O_5 and then K_2CO_3, and passed through an Al_2O_3 column (diameter: 2 cm, length: 15 cm; neutral alumina, dried at 140 °C and cooled under argon).

Tetra-*n*-butylammonium hexafluorophosphate, NBu_4PF_6, was prepared from NBu_4Br and NH_4PF_6 or recycled as described before.[51] It was used in a concentration of 0.1 M.

The electrolyte was degassed by three freeze–pump–thaw cycles before it was transferred into the electrochemical cell under argon.

All electrochemical experiments were performed with a Bioanalytical Systems (BAS, West Lafayette, IN, USA) 100 B/W electrochemical workstation controlled *via* a standard 80486 personal computer (control program version 2.0). For electroanalytical experiments a Pt electrode tip of Metrohm (Filderstadt, Germany) was used as working electrode. The electroactive area of the Pt disk was determined from cyclic voltammograms, chronoampero- and -coulograms of fc in

acetonitrile, CH_2Cl_2 and a 1 : 1 (v/v) mixture of these solvents to be $A = 0.071 \pm 0.007$ cm², using diffusion coefficients D for fc in CH_3CN (2.4×10^{-5} cm² s^{-1})[52] and CH_2Cl_2 (2.32×10^{-5} cm² s^{-1}).[53] The value of D in the solvent mixture was calculated as the mean value of the values in the pure solvents. The counter electrode was a Pt wire of 1 mm diameter. A single-unit Haber–Luggin double-reference electrode[54] was used. The resulting potential values refer to Ag/Ag^+ (0.01 M in CH_3CN–0.1 M NBu_4PF_6). Ferrocene was used as an external standard. Its potential was determined by separate cyclic voltammetric experiments, and all potentials were then rescaled to E^0 (fc/fc^+) = +0.211 V *vs*. Ag/Ag^+. All potentials in the present paper are given relative to this standard.[24]

For cyclic voltammetry a gas-tight full-glass three-electrode cell was used, whose assembly for the experiments was described previously.[51] The cell was purged with argon prior to filling it with electrolyte. Background curves were recorded before adding substrate to the solution. These were later subtracted from the experimental data with substrate. The automatic BAS 100 B/W *iR*-drop compensation facility was used for all experiments.

HBF_4 was 54% in diethyl ether (Fluka, Buchs, Switzerland) and was transferred into the electrochemical cell with a syringe.

For preparative electrolyses working and counter electrodes were nets of Pt/Ir, 90/10 (Degussa, Hanau, Germany). They were separated from each other by a glass frit. The reference electrode was identical to the one described above. The cell was fitted with an additional Pt tip electrode (see above) to record cyclic voltammograms in the electrolyte. This cell was also gas-tight and could be thermostatted. It was purged with argon prior to filling it with electrolyte.

Numerical simulations[48] were performed with the commercial DigiSim software (BAS; FIFD algorithm, default numerical options).[55] Semi-infinite planar diffusion was assumed. The pre-equilibrium option of the program was enabled for chemical equilibria only. The temperature was set to 298.2 K, all transfer coefficients of the electron transfers were assumed to be 0.5, while both the uncompensated resistance and the double layer capacity were set to zero in the simulations.

Acknowledgements

Financial support by the Deutsch Forschungsgemeinschaft and by the Fonds der Chemischen Industrie is gratefully acknowledged. We are indebted to Professor Dr Hartmut B. Stegmann for helpful discussions and to Paul Schuler for EPR measurements.

References

1 For an overview see A. R. Katritzky and C. W. Rees (Eds.), *Comprehensive Heterocyclic Chemistry*, Vol. 4, Pergamon, Oxford, 1984; R. A. Jones, *Pyrroles (The Chemistry of Heterocyclic Compounds)*, John Wiley & Sons, New York, 1990/1992; A. R. Katritzky, C. W. Rees and E. F. V. Scriven, *Comprehensive Heterocyclic Chemistry II*, Vol. 2, Pergamon, Oxford, 1996.
2 R. Kuhn and H. Kainer, *Biochim. Biophys. Acta*, 1953, **12**, 325; S. M. Blinder, M. L. Peller, N. W. Lord, L. C. Aamodt and N. S. Ivanchukov, *J. Chem. Phys.*, 1962, **36**, 540; R. A. Allendoerfer and A. S. Pollock, *Mol. Phys.*, 1971, **22**, 661.
3 H. Zimmermann, H. Baumgärtel and F. Bakke, *Angew. Chem.*, 1961, **73**, 808; K. Schilffarth and H. Zimmermann, *Chem. Ber.*, 1965, **98**, 3124.
4 M. R. C. Gerstenberger, A. Haas, B. Kirste, C. Krüger and H. Kurreck, *Chem. Ber.*, 1982, **115**, 2540.
5 W. Flitsch, H. Peeters, W. Schulten and P. Rademacher, *Tetrahedron*, 1978, **34**, 2301; E. Orti, J. Sanchez-Marin, P. M. Viruela-Martin and F. Tomas, *Chem. Phys. Lett.*, 1986, **130**, 285; W. M. F. Fabian, *J. Comput. Chem.*, 1988, **9**, 369.
6 See *e.g.* W. Flitsch and H. Peeters, *Chem. Ber.*, 1973, **106**, 1731; W. Flitsch and H. Peeters, *Chem. Ber.*, 1977, **110**, 273.
7 For an overview see: N. Kuhn, *Bull. Soc. Chim. Belg.*, 1990, **99**, 707; Ch. Janiak and N. Kuhn, *Advances in Nitrogen Heterocycles*, Vol. 2, pp. 179–210, JAI Press, Greenwich, Connecticut, 1996.
8 W. A. Jung, Dissertation, Universität Gießen, 1982, ref. in G. Maier, N. H. Wiegand, S. Baum, R. Wüllner, W. Mayer and R. Boese, *Chem. Ber.*, 1989, **122**, 767.
9 See *e.g.* N. Kuhn, E.-M. Horn, E. Zauder, D. Bläser and R. Boese, *Angew. Chem.*, 1988, **100**, 572; *Angew. Chem., Int. Ed. Engl.*, 1988, **27**, 579; N. Kuhn, M. Schulten, E. Zauder, N. Augart and R. Boese, *Chem. Ber.*, 1989, **122**, 1891; N. Kuhn, A. Kuhn and E.-M. Lampe, *Chem. Ber.*, 1991, **24**, 997; N. Kuhn, J. Kreutzberg, E.-M. Lampe, D. Bläser and R. Boese, *J. Organomet. Chem.*, 1993, **458**, 125.
10 G. Korschun, *Ber. Dtsch. Chem. Ges.*, 1904, **37**, 2183; C. Chang and R. Adams, *J. Am. Chem. Soc.*, 1931, **53**, 2353.
11 See *e.g.* W. Flitsch, U. Krämer and H. Zimmermann, *Chem. Ber.*, 1969, **102**, 3268; W. Flitsch and W. Schulten, *Synthesis*, 1977, 414.
12 N. Kuhn, E.-M. Horn and E. Zauder, *Inorg. Chim. Acta*, 1988, **149**, 163.
13 D. V. Avila and A. G. Davies, *J. Chem. Soc., Faraday Trans.*, 1990, **86**, 3243.
14 N. Kuhn, E.-M. Horn, R. Boese and N. Augart, *Angew. Chem.*, 1988, **100**, 1433; *Angew. Chem., Int. Ed. Engl.*, 1988, **27**, 1368.
15 N. Kuhn and H. Kotowski, unpublished results.
16 A. Grimison and G. A. Simpson, *J. Phys. Chem.*, 1968, **72**, 1176.
17 M. Shiotani, Y. Nagata, M. Tasaki, J. Sohma and T. Shida, *J. Phys. Chem.*, 1983, **87**, 1170.
18 D. N. R. Rao and M. C. R. Symons, *J. Chem. Soc., Perkin Trans. 2*, 1983, 135.
19 A. G. Davies, L. Julia and S. N. Yazdi, *J. Chem. Soc., Chem. Commun.*, 1987, 929; D. V. Avila and A. G. Davies, *J. Chem. Soc., Perkin Trans. 2*, 1991, 1111.
20 K. Tanaka, T. Nomura, T. Noro, H. Tatewaki, T. Takada, H. Kashigawi, F. Sasaki and K. Ohno, *J. Chem. Phys.*, 1977, **67**, 5738; C. Aleman, M. C. Vega and J. J. Perez, *J. Mol. Struct. (THEOCHEM)*, 1993, **281**, 39.
21 Y. Chiang and E. B. Whipple, *J. Am. Chem. Soc.*, 1963, **85**, 2763; F. G. Terrier, F. L. Lebleds, J. F. Verchere and A. P. Chatrousse, *J. Am. Chem. Soc.*, 1985, **107**, 307; F. Terrier, A.-P. Chatrousse, J. R. Jones, S. W. Hunt and E. Buncel, *J. Phys. Org. Chem.*, 1990, **3**, 684; Y. Nakajima, Y. Sakagishi, M. Shiibashi, Y. Suzuki and H. Kato, *J. Mol. Struct. (THEOCHEM)*, 1993, **288**, 199.
22 E. E. Havinga, K. H. Boswijk and E. H. Wiebenga, *Acta Crystallogr.*, 1954, **7**, 487.
23 A strongly distorted geometry has been observed for the I_8^{2-} ion of the $[(CH_2)_6N_4CH_3]_2$ salt: P. K. Hon, T. C. W. Mak and J. Trotter, *Inorg. Chem.*, 1979, **10**, 2916.
24 G. Gritzner and J. Kůta, *Pure Appl. Chem.*, 1984, **56**, 461.
25 A. Smie and J. Heinze, *Angew. Chem.*, 1997, **109**, 375; *Angew. Chem., Int. Ed. Engl.*, 1997, **36**, 363.
26 A. Merz, J. Kronberger, L. Dunsch, A. Neudeck, A. Petr and L. Parkanyi, *Angew. Chem.*, 1999, **111**, 1533; *Angew. Chem., Int. Ed. Engl.*, 1999, **38**, 1442.
27 J. M. Savéant and E. Vianello, *Electrochim. Acta*, 1967, **12**, 1545.
28 J. Phelps and A. J. Bard, *J. Electroanal. Chem.*, 1976, **68**, 313.
29 S. Dümmling, B. Speiser, N. Kuhn and G. Weyers, *Acta Chem. Scand.*, 1999, **53**, 876.
30 K. Hesse, S. Hünig and H. Wenner, *Liebigs Ann. Chem.*, 1982, 2079.
31 D. H. Evans and K. Hu, *J. Chem. Soc., Faraday Trans.*, 1996, **92**, 3983.
32 S. F. Nelsen, *Acc. Chem. Res.*, 1981, **14**, 131.
33 S. F. Nelsen, *Adv. Electron Transfer Chem.*, 1993, **3**, 167.
34 S. F. Nelsen, L.-J. Chen, P. A. Petillo, D. H. Evans and F. A. Neugebauer, *J. Am. Chem. Soc.*, 1993, **115**, 10611.
35 S. F. Nelsen, L.-J. Chen, M. T. Ramm, G. T. Voy, D. R. Powell, M. A. Accola, T. R. Seehafer, J. J. Sabelko and J. R. Pladziewicz, *J. Org. Chem.*, 1996, **61**, 1405.
36 M. Dietrich, J. Heinze, H. Fischer and F. A. Neugebauer, *Angew. Chem.*, 1986, **98**, 999; *Angew. Chem., Int. Ed. Engl.*, 1986, **25**, 1021.
37 M. Dietrich, J. Heinze, C. Krieger and F. A. Neugebauer, *J. Am. Chem. Soc.*, 1996, **118**, 5020.
38 S. F. Nelsen, S. C. Blackstock and K. J. Haller, *Tetrahedron*, 1986, **42**, 6101.
39 K. Deuchert and S. Hünig, *Angew. Chem.*, 1978, **90**, 927; *Angew. Chem., Int. Ed. Engl.*, 1978, **17**, 875.
40 M. Schmittel and A. Burghart, *Angew. Chem.*, 1997, **109**, 2658; *Angew. Chem., Int. Ed. Engl.*, 1997, **36**, 2550.
41 N. G. Connelly and W. E. Geiger, *Chem. Rev.*, 1996, **96**, 877.
42 L. K. Bieniasz, S. Dümmling, B. Speiser and M. Würde, *J. Electroanal. Chem.*, 1998, **447**, 173.
43 R. F. Dapo and C. K. Mann, *Anal. Chem.*, 1963, **35**, 677.
44 C. D. Russell, *Anal. Chem.*, 1963, **35**, 1291.

45 K. L. Handoo, J.-P. Cheng and V. D. Parker, *Acta Chem. Scand.*, 1993, **47**, 626.
46 J. M. Savéant and E. Vianello, *Electrochim. Acta*, 1963, **8**, 905.
47 P. Hertl and B. Speiser, *J. Electroanal. Chem.*, 1988, **250**, 237.
48 B. Speiser, in *Electroanalytical Chemistry*, eds. A. J. Bard and I. Rubinstein, Vol. 19, Marcel Dekker, New York, 1996, pp. 1–108.
49 W. Luo, S. W. Feldberg and M. Rudolph, *J. Electroanal. Chem.*, 1994, **368**, 109.
50 K. G. Hancock and P. L. Wylie, *J. Org. Chem.*, 1977, **42**, 1850.
51 S. Dümmling, E. Eichhorn, S. Schneider, B. Speiser and M. Würde, *Curr. Sep.*, 1996, **15**, 53.
52 T. Kuwana, D. E. Bublitz and G. Hoh, *J. Am. Chem. Soc.*, 1960, **82**, 5811.
53 J. B. Cooper and A. M. Bond, *J. Electroanal. Chem.*, 1991, **315**, 143.
54 B. Gollas, B. Krauß, B. Speiser and H. Stahl, *Curr. Sep.*, 1994, **13**, 42.
55 M. Rudolph, D. P. Reddy and S. W. Feldberg, *Anal. Chem.*, 1994, **66**, 589A.
56 R. S. Nicholson, *Anal. Chem.*, 1966, **38**, 1406.

Paper 9/05603C